

## Supporting Information

### **Droplet-templating into structured bead-based aerogels with compartmentalized or welded configurations**

Shayan Ghasemi<sup>1</sup>, Mahyar Panahi<sup>2</sup>, Elnaz Erfanian<sup>1,3</sup>, Tianyu Guo<sup>3</sup>, Vahid Rad<sup>4</sup>, Adel Jalaei<sup>3</sup>, Gabriel Banvillet<sup>3</sup>, E. Johan Foster<sup>3</sup>, Kam C. Tam<sup>1</sup>, Masoud Soroush<sup>4</sup>, Feng Jiang<sup>3</sup>, Orlando J. Rojas<sup>2,3,5</sup>, Milad Kamkar<sup>1\*</sup>

<sup>1</sup> Department of Chemical Engineering, Waterloo Institute for Nanotechnology, University of Waterloo, 200 University Avenue West, Waterloo, Ontario N2L 3G1, Canada

<sup>2</sup> Department of Wood Science, The University of British Columbia, 2900-2424 Main Mall Vancouver BC V6T 1Z4, Canada

<sup>3</sup> BioProducts Institute and Department of Chemical and Biological Engineering, University of British Columbia, 2360 East Mall, Vancouver BC V6T 1Z3, Canada

<sup>4</sup> Department of Chemical and Biological Engineering, Drexel University, Philadelphia, PA 19104, USA

<sup>5</sup> Department of Chemistry, 2036 Main Mall, The University of British Columbia, Vancouver BC V6T 1Z1, Canada

**\*Corresponding Author:** [Milad.kamkar@uwaterloo.ca](mailto:Milad.kamkar@uwaterloo.ca)

## 1. Experimental Section

### 1.1 Materials

Cellulose nanocrystal (CNC) was provided from CelluForce Inc. Hexane (#107-83-5), PSS-[3-(2-aminoethyl) amino] propyl-heptaisobutyl substituted POSS (POSS- $NH_2$ ), sulfuric acid ( $H_2SO_4$ , 95-98 wt.%), hydrogen peroxide ( $H_2O_2$ , 30 wt.%), and TEMPO (2,2,6,6-tetramethylpiperidine-1-oxyl), were all purchased from Sigma-Aldrich. Potassium permanganate (Anachemia, Reagent Grade, 99%) was used in this work. The optimized MAX phase, titanium aluminum carbide ( $Ti_3AlC_2$ ), used for synthesizing  $Ti_3C_2T_x$  MXene flakes, was kindly provided by Prof. B. Anasori at Purdue University [1]. Hydrochloric acid (HCl, 37 wt%) and hydrofluoric acid (HF, 49-51 wt.%) for the synthesis, and lithium chloride (LiCl, 99.98%) for delamination, were purchased from Fisher Scientific and Alfa Aesar, respectively. Also, sodium bromide (NaBr), sodium hypochlorite (NaOCl) and sodium hydroxide (NaOH) were received from Sigma-Aldrich. All chemicals were used as received without further purification. Deionized water was used in all the experiments.

### 1.2 Droplet-Templating

Soft materials are prepared by extruding the aqueous phase into the oil phase using a BIO X 3D printer equipped with dispensing needles with different diameters. The size and shape of the produced droplets are controlled by various factors such as injection pressure and needle diameter.

### 1.3 GO Synthesis and Characterization

Graphene oxide (GO) was synthesized through a previously discussed method [2]. Graphite powder (Asbury Carbon, Natural Flake) and sodium nitrate (Sigma-Aldrich, ReagentPlus,  $\geq 99\%$ ) were mixed in a 2:1 ratio with concentrated sulfuric acid in an ice bath. Potassium permanganate was then gradually added at a 3:1 ratio ( $KMnO_4$ :graphite) under vigorous stirring, maintaining the temperature below 20 °C. The reaction mixture was then stirred at 35 °C until a brownish paste formed. To control the temperature below 50 °C, the mixture was gradually diluted with deionized water in an ice bath. Subsequently, a hydrogen

peroxide solution in deionized water was added, and the suspension was stirred for 2 hours. After centrifugation, the solids were washed with an HCl-containing aqueous solution to remove residual ions, followed by multiple rinses with deionized water. The resulting graphite oxide was exfoliated in water using bath sonication. Finally, large unexfoliated solids were separated from GO via centrifugation at 4000 rpm. Check ref [2] for additional information.

#### **1.4 MXene Synthesis and Characterization**

Well-exfoliated  $Ti_3C_2T_x$  flakes were synthesized via mild etching of the MAX phase with an average particle size of  $\sim 75 \mu m$ . In brief, 2 g of MAX phase was gradually added (over 5 minutes) to a mixture of 18 mL deionized (DI) water, 36 mL of 12 M HCl, and 6 mL of 29 M HF. The mixture was stirred at 400 rpm for 24 hours at 35 °C. The resulting etched solution was washed with DI water via centrifugation at 5000 rpm for 5 minutes until the supernatants reached a pH of 6. To delaminate the  $Ti_3C_2T_x$  flakes, the multilayered  $Ti_3C_2T_x$  sediments were added to 100 ml of 0.5 M LiCl solution. The mixture was stirred at 400 rpm for 1h at 65 °C under argon gas. Multilayer flakes or unreacted material were separated from the well-exfoliated flakes by centrifugation at 5000 rpm for 10 minutes for 3 cycles. After that, the suspension was centrifuged at 3000 rpm for 30 minutes to collect the supernatant as the final  $Ti_3C_2T_x$  MXene suspension. Check reference [1] for additional information.

#### **1.5 CNF Synthesis and Characterization**

TEMPO-oxidized cellulose nanofibers were synthesized from 10 g of refined bleached eucalyptus kraft fibers (dry equivalent) through a TEMPO-mediated oxidation process. The reaction was carried out using a TEMPO/NaBr/NaClO system at a molar ratio of 0.1 mmol:1 mmol:5 mmol per gram of fiber. Check reference [3] for additional information and detailed synthesis procedure and characterization.

## **2. Exploiting Self-Assembly to Create Interfacial Layers**

Building upon the understanding of GO assembly and layer formation at the interface, we explore similar mechanisms for three additional nanomaterials: CNC, CNF, and MXene.

*CNF fibrils, 1D.* Despite their structures, e.g., 2D for GO versus fiber/rod-shaped 1D for CNF and CNC, the assembly and jamming mechanisms for all nanomaterials display similarities. This study employs TEMPO-oxidized cellulose nanofibers (CNF for short), which incorporates carboxylic acid groups onto the CNF surface. Hence, the rationale behind the assembly of CNF is similar to GO flakes due to CNF amphiphilic nature. The CNF/POSS- $NH_2$  co-assembly process is likely driven by the complexation between the deprotonated carboxylic acid groups ( $COO^-$ ) and the positively charged amine groups ( $NH_3^+$ ) of POSS- $NH_3^+$ , leading to the minimization of interfacial energy and jamming at the interface. The jamming occurs when CNF adsorbs tightly at the oil/water interface, forming a solid-like film. This jamming phenomenon is facilitated by the addition of POSS- $NH_2$ , which screens charges on the fibrils and weakens electrostatic repulsion barriers between the fibers, allowing for rapid accumulation and jamming of the CNF at the interface.

*Rod-like CNC, 1D.* Also, this research utilizes CNCs functionalized with sulfate groups and these negatively charged groups prevent aggregation, yielding well-dispersed CNCs in water. Surfactants containing primary amine groups dissolved in hexane migrate to the interface between the hexane and water. The interfacially assembled positive POSS- $NH_3^+$  attracts the negatively charged sulfate groups on the CNCs, leading to the co-assembly of a nanoparticles-surfactants (NPSs) layer around the water droplet. This interactions between sulfate groups and the positively charged amine groups ( $NH_3^+$ ) of POSS- $NH_3^+$  acts as a bridge, attracting the CNCs towards the hexane-water interface. CNCs in proximity to the interface migrate towards it, the POSS- $NH_3^+$  anchor them at the water-hexane interface. This combination of CNCs and surfactant tethered at the interface forms an NPSs layer. When the interfacial area between the two liquids is reduced, the NPSs become increasingly crowded at the interface, which restricts their movement, leading to a jammed state, which is crucial for stabilizing the interface.

*MXenes, 2D.* A fourth class of nanomaterials, 2D MXenes, exhibits remarkable potential for interfacial engineering. Similar to the interaction observed between GO and POSS- $NH_3^+$ , negatively charged  $Ti_3C_2T_x$

MXene flakes participate in the assembly at the interface. Due to the abundance of negatively charged functional groups like  $F^-$ , and  $O^-$  on their surface,  $Ti_3C_2T_x$  flakes electrostatically interact with the protonated  $POSS-NH_3^+$  at interfacial layer. This interaction drives the formation of overlapping  $Ti_3C_2T_x$ -POSS NPSs complexes. As the  $Ti_3C_2T_x$ -POSS complex forms at the interface,  $Ti_3C_2T_x$  nanosheets become increasingly crowded due to limited space. This crowding restricts the movement and rearrangements of the NPSs units, leading to a jammed state. This jamming forms a dense and robust assembly at the interface, resembling a solid-like layer and stabilizing the liquid droplets containing  $Ti_3C_2T_x$ .

### 3. Supplementary Figures

#### Visualization of GO aerogel beads

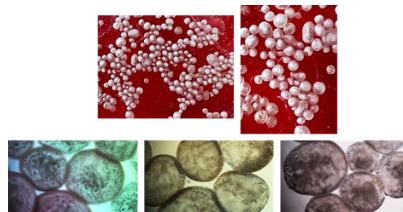


**Figure S1.** Aerogel beads of GO, digital images and optical microscope graphs.

#### Dispersibility and Liquid-like Behavior of Nanomaterials in Aqueous Suspensions

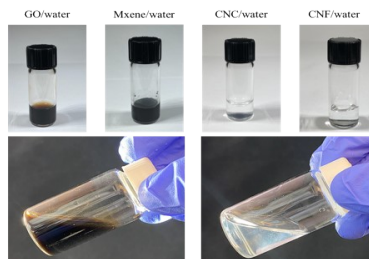


**Figure S2.** Aqueous suspensions of GO, MXene, CNC, and CNF. The second row shows their liquid-like nature.

#### Droplet formation

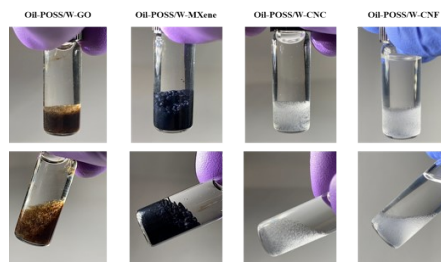
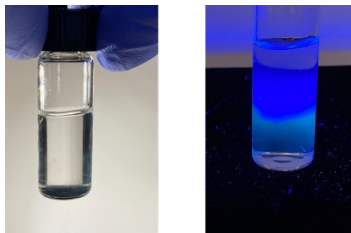


**Figure S3.** Fabricated droplet templates after jetting GO, MXene, CNC, CNF suspensions in hexane/POSS phase.

### Fluorescently Labeled Compartmentalized All-aqueous CNC Suspension



**S4.** Digital image of a successfully compartmentalized all-aqueous 1wt.% CNC suspension. The top layer is labeled with a fluorescent dye for clarity.

### Tailoring CNC Droplet Size via Jetting Conditions

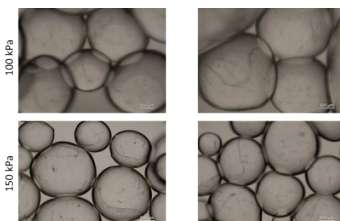


**Figure S5.** Influence of jetting conditions on CNC droplet size. The image shows a series of CNC droplets produced under different jetting conditions, with variations in droplet size evident.

### Tailoring MXene Droplet Size via Jetting Conditions



**Figure S6.** Influence of jetting conditions on MXene droplet size. The image shows a series of MXene droplets produced under different jetting conditions, with variations in droplet size evident.

### Directed Assembly of Magnetic GO Droplets into Macrostructures



**Figure S7.** GO droplets loaded with magnetic particle organized in letter shape.

### References

1. Thakur A. *Small Methods*, 2023;7 (8): 2300030.
2. Kamkar M, et al. *Advanced Materials and Interfaces* 2022;**9**:2101659.
4. Banvillet G, et al. *Materials Today Nano* 2023, **24**: 100424.